

Electrochemical characterization of nickel hydroxide nanomaterials as electrodes for Ni-MH batteries

S. G. Real¹ · M. G. Ortiz^{1,2} · E. B. Castro¹

Received: 20 April 2016 / Revised: 28 July 2016 / Accepted: 2 August 2016 / Published online: 23 August 2016
© Springer-Verlag Berlin Heidelberg 2016

Abstract β -Nickel hydroxide was successfully synthesized by a hydrothermal method. Nano-nickel hydroxide material was characterized by X-ray diffraction, infrared absorption spectroscopy, and transmission electron microscopy. They were employed as additives to the positive electrode of Ni-MH batteries. Working electrodes, with mixtures of commercial nickel hydroxide and nano-nickel hydroxide (0–10 wt.%) as active material, were prepared. Cyclic voltammetry, charge/discharge profiles, and electrochemical impedance spectroscopy studies were carried out to evaluate the electrochemical performance of the nickel electrode, in 7 M KOH electrolyte, at 25 °C. The presence of nano-nickel hydroxide improves the electrochemical behavior of the active material. The electrochemical impedance spectroscopy (EIS) results were analyzed employing a modified version of previously developed physicochemical model that takes into account the main structural and physicochemical parameters that control these systems.

Keywords Hydrothermal synthesis · Nano-nickel hydroxide · Positive electrodes · Ni-MH batteries · Electrochemical characterization

Castro E.B. passed away on 18th February 2013.

✉ S. G. Real
sreal@inifta.unlp.edu.ar

✉ M. G. Ortiz
mortiz@inifta.unlp.edu.ar

¹ Instituto de Investigaciones Fisicoquímicas Teóricas y Aplicadas (INIFTA), Facultad de Ciencias Exactas, Universidad Nacional de La Plata, C.C.16, Suc. 4, (1900), La Plata, Argentina

² Centro de Investigación, Desarrollo en Ciencia y Tecnología de los Materiales (CITEMA), Facultad Regional La Plata, Universidad Tecnológica Nacional, Calle 60 y 124, La Plata, Argentina

Introduction

In the last decades, there has been much interest focused on the development of devices as alternative energy sources. Among them, alkaline rechargeable batteries such as Ni-MH and Ni-Cd are widely employed in today's market, covering domains ranging from power tools to portable electronics and electric vehicles. In these alkaline batteries, the positive electrode is the nickel hydroxide active material. Consequently, there has been a scientific and technological interest in studying the electrochemical behavior of nickel hydroxide electrodes. Particularly, for further battery applications, the improvement in some Ni(OH)₂ properties are required, i.e., nickel hydroxide products with good crystallinity, homogeneity, uniform morphology distribution, with nanometer size particles and high surface area [1–4].

Since the 1990s, increasing interest has been focused on nanoscale science and technology in the field of chemical power sources. Nanomaterials, exhibit physical and chemical properties different from those of conventional bulk; for example, lower diffusion activation energy of nanostructured materials and thus, larger diffusion coefficient than in the corresponding bulk counterpart can be found [5].

Furthermore, in the case of nanomaterials for lithium batteries, it has been reported that reduced particle sizes can cause changes in the thermodynamics of the reaction [6], a significant increase of the ion insertion/removal rate, due to short distances for ion transport within the particle, and also the enhancement of the electron transport process [7].

Due to all these facts, the use of nanomaterials in battery electrodes offers the potential of improving performance in terms of charge-storage capacity, rate capability, and cycle life. In order to improve the conductivity and reversibility of the charge/discharge processes, and to enhance the specific charge capacity, many studies have been carried out by

incorporating additives (i.e., Al, Zn, Cd, Co) [8–11] and nanomaterials [1–5, 12, 13]. Furthermore, the performance (i.e., discharge capacity) of positive electrodes of nickel batteries is highly dependent on the size, morphology, composition, and phase of nickel hydroxide-active material [14–16]. There are synthesis methods that employ a template to control these last characteristics. However, the hydrothermal synthesis is a low-cost and simple method that allows obtaining controllable nanostructures [17, 18] and that can be used for large-scale production of Ni(OH)₂.

In some works, hydrothermal synthesis method has been employed to obtain active nanomaterials for supercapacitors and electrocatalytic purposes, but there are not many investigations related to active nanomaterials for battery electrode applications [19].

In this paper, the synthesis of nano-nickel hydroxide obtained by a hydrothermal treatment is reported. The prepared samples were characterized by powder X-ray diffraction (XRD), infrared absorption spectroscopy (IR), and transmission electron microscopy (TEM). The effects of different weight percent contents of nano-nickel hydroxide added to positive electrodes of Ni-MH batteries have been investigated using cyclic voltammetry (CV), charge/discharge, and electrochemical impedance spectroscopy (EIS) techniques.

The EIS results of prepared samples were analyzed employing a modified version of the previously developed physicochemical model [8, 11, 13, 20–22].

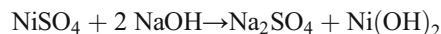
The aim in the present paper is to study the electrochemical behavior of different weight percent contents of nano-nickel hydroxide material added to nickel-positive electrodes and to model EIS results taking into consideration the main structural and physicochemical parameters that control these systems.

Experimental Aspects

All the reagents used in the synthesis of nano-nickel hydroxide were of analytical grade and employed without further purification. Ni(OH)₂ was synthesized by a hydrothermal process as follows (Fig. 1): 20 ml of 1.6 M NaOH solution was slowly added to 20 ml of 0.8 M NiSO₄·6H₂O solution. Then, this mixed solution was loaded into Teflon-lined stainless steel autoclave. During the heating process (from room temperature to 180 °C), the homogeneous nucleation process (nanoparticles) initially occurs, leading to particle growth. Their sizes depend on the aging time of the precipitate. Thus, the synthesized product begins to grow and coalesce to form aggregated particles (schematic representation of the materials formation process is shown in Fig. 1). The autoclave was maintained at 180 °C at different times: 4, 12, and 24 h (named as β-Ni(OH)₂-4, β-Ni(OH)₂-12, and β-Ni(OH)₂-24, respectively). After this procedure, a green suspension in aqueous solution was obtained; this product was filtered and

washed with deionized water followed by drying at 70 °C for 24 h.

The formation of nickel hydroxide takes place through a simple chemical reaction:



The chemical composition, crystalline phase, and morphology of synthesized powder were characterized by X-ray powder diffraction (XRD; Model PW-1730, Philips) with CuKα radiation ($\lambda = 1.54178 \text{ \AA}$), infrared spectroscopy (IRAffinity-1 SHIMADZU Fourier transform infrared spectrophotometer), using KBr from 4000 to 400 cm⁻¹, and transmission electron microscopy (TEM; Model JEM-1200EX II, Jeol Co, Japan).

In this work, β-Ni(OH)₂-4 materials were used as additives to nickel-positive electrodes. The electrode slurry was prepared by mixing active material (Ni(OH)₂, Aldrich), 35 wt.% teflonized carbon (Vulcan XC-72R + 30 % PTFE), and different amounts of β-Ni(OH)₂-4 previously synthesized, as follows:

- 0 wt.% β-Ni(OH)₂-4, Ni-0 electrode;
- 2 wt.% β-Ni(OH)₂-4, Ni-2 electrode;
- 5 wt.% β-Ni(OH)₂-4, Ni-5 electrode;
- 10 wt.% β-Ni(OH)₂-4, Ni-10 electrode.

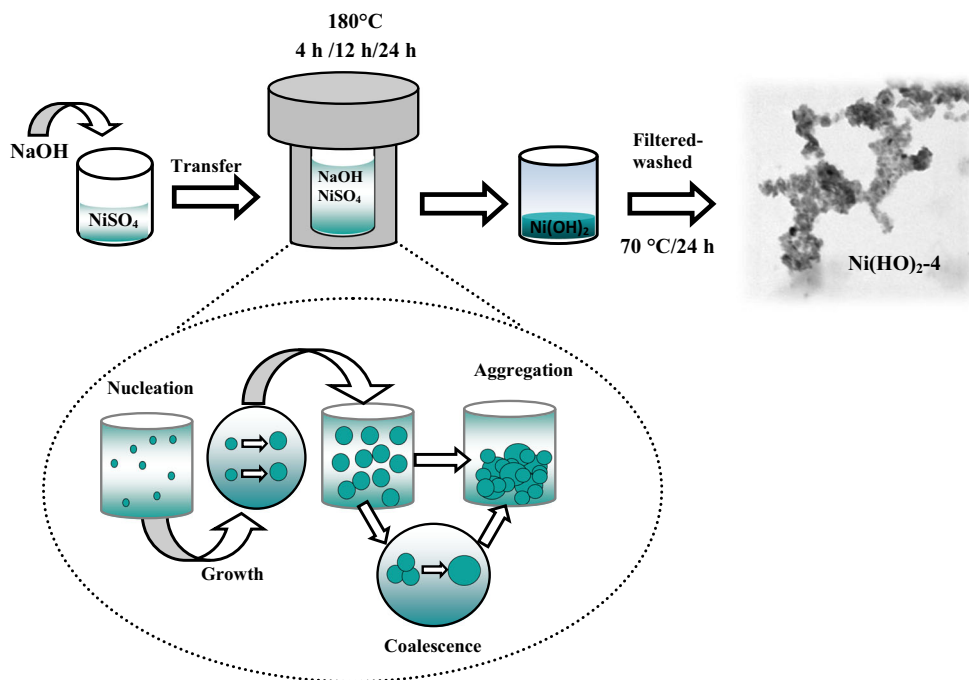
The obtained slurry was pasted onto a nickel foam substrate (Goodfellow Ni003851/1). The area of working electrodes was 0.4 cm² and the thickness, 80 μm.

Electrochemical measurements were performed in a three-compartment cell, with the corresponding working electrode, counter electrode (nickel mesh of large specific area), and reference electrode (Hg/HgO_{ss}); all cell compartments were immersed in the electrolyte 7 M KOH solution. The experiments were carried out at 30 °C. The potential values in the text are referred to the Hg/HgO_{ss} electrode.

Cyclic voltammetry (CV), constant current charge/discharge, and electrochemical impedance spectroscopy (EIS) measurements were performed using a PAR potentiostat and a Schlumberger 1250 frequency response analyzer. The CVs were measured at a scanning rate of 5 mV s⁻¹ with the voltage limits ranging from 0.05 to 0.55 V. In the constant current charge/discharge curves, the discharge cut-off potential was set at 0.2 V.

Before each EIS experiment, the working electrodes were previously activated by electrochemical cycles, by charging at a current corresponding to C/2 and discharging at the same current, until a constant capacity was reached. Then, the electrodes were discharged galvanostatically up to 60 % state of discharge (SOD) and the EIS measurements were carried out potentiostatically at the open-circuit potential. EIS spectra were recorded between 20 kHz and 50 mHz employing a low

Fig. 1 Schematic illustration of sequential steps for the synthesis of β -Ni(OH)₂



amplitude sine wave potential signal (5 mV) superimposed on the polarization potential.

The morphology of electrode surfaces was characterized by scanning electron microscopy, Philips SEM Model 505, with a Soft Imaging System ADDA II.

Results and discussion

Powder characterization

XRD patterns of the samples obtained by the hydrothermal method are shown in Fig. 2. The samples present characteristic peaks at 2θ values equal to 19.3°, 33.1°, and 38.5°. They can be ascribed to the crystal structure typical of β -Ni(OH)₂ with a brucite-type structure and a hexagonal unit where these characteristic peaks are related to [001], [100], and [101] crystal planes, respectively (JCPDS-14-0117), in agreement with previous reports [2, 17, 23].

No peaks from the precursors or any other phases were observed, which indicates that the utilized hydrothermal conditions are favorable for the formation of pure β -Ni(OH)₂. Therefore, the prepared products are the typical active materials usually used for nickel hydroxide electrodes in nickel-metal hydride batteries.

All reflections exhibit different width and intensity. It has been reported in the literature that the width of the diffraction lines corresponding to (20 ℓ) and (10 ℓ) with $\ell \neq 0$ are related to the presence of stacking faults [24, 25]. For example, an abnormal enlargement of reflections [101] and [102] is characteristic of the presence of stacking faults in the nickel

hydroxide structure [26]. As a first approximation, like many authors in the literature [26, 27], the crystal size (d) can be estimated by XRD using Scherrer's formula [28–30]. Accordingly, the β -Ni(OH)₂ crystal sizes are derived from the basal plane [001] and the obtained values are presented in Table 1. The experiments were repeated three times, and in all cases, the corresponding experimental error was lower than 10 %.

The β -Ni(OH)₂-4 materials exhibited the smallest crystal size (Table 1), and consequently, they were selected as additive to prepare the positive electrodes of Ni-MH batteries.

Figure 3 depicts that the IR spectra of commercial and synthesized powders are very similar. These results confirm

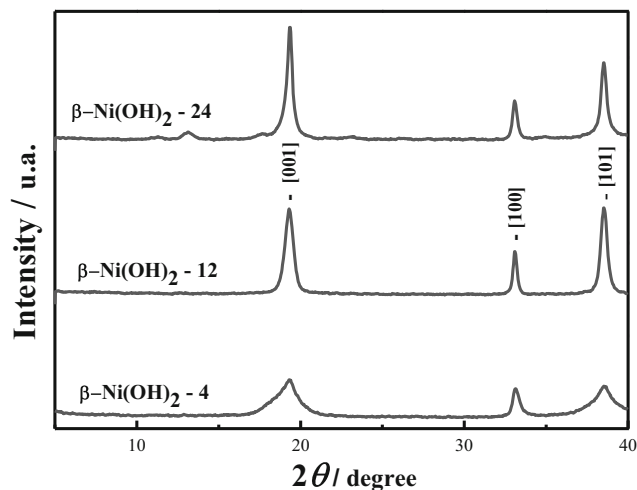


Fig. 2 XRD patterns of the materials prepared by the hydrothermal method

Table 1 Crystal size calculated from XRD

Sample	Crystal size (nm)
β -Ni(OH) ₂ -4	14
β -Ni(OH) ₂ -12	58
β -Ni(OH) ₂ -24	52

the existence of the β -Ni(OH)₂ phase due to the presence of a sharp and narrow band around 3643, 520, and 450 cm⁻¹, corresponding to ν (OH), ν Ni–OH, and ν Ni–O stretching vibrations, respectively [18, 31].

Other peaks were observed at 3440 cm⁻¹, related to the vibrational stretching of the hydroxyl group of adsorbed water, and at 1630 cm⁻¹, assigned to the vibration of water molecules [31, 32].

Absorption bands located in the 800–1800-cm⁻¹ range could be due to the presence of anions (carbonates (1450 cm⁻¹), nitrates (1380 cm⁻¹), and sulfates (1042 cm⁻¹) [31–33]).

Figure 4 shows the TEM images of the materials synthesized. It can be seen that the hydroxide precipitate is formed by agglomeration of particles in the nanometer size. The morphologies of β -Ni(OH)₂ changed with the hydrothermal time; when the reaction time was less than 12 h, the product appears as aggregates (clusters whose total size exceeds the nanometric dimensions). The elongation of products can be observed at longer synthesis time. The formation of nanoribbons was seen at 24 h reaction time (Fig. 4c) when, almost exclusively, a large number of ribbon-like nanostructures are shown. The nanoribbons had typical thicknesses and widths in the nanometer size range. Therefore, the formation of nanoribbons can be explained considering that longer hydrothermal reaction time resulted in the overgrowth of agglomerates (Fig. 4a, b). These reaction

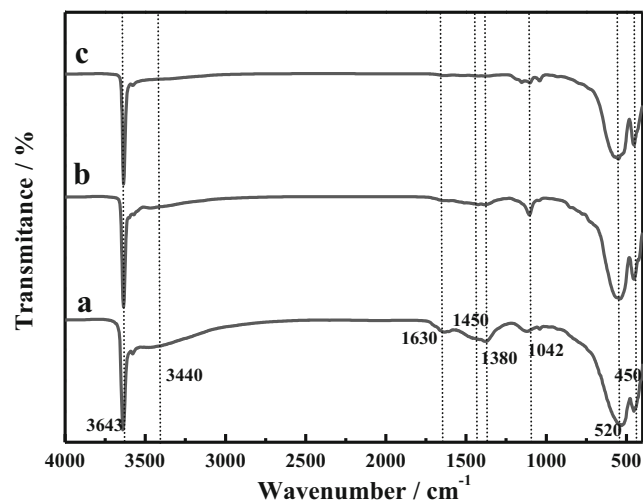


Fig. 3 IR spectra of samples: **a** β -Ni(OH)₂-4; **b** β -Ni(OH)₂-12; **c** β -Ni(OH)₂-24

products, for increasing synthesis time, cannot endure the pressure of autoclave and smashed into nanoribbons (Fig. 4c).

SEM analysis

The electrode surfaces were studied by SEM. The micrographs are presented in Fig. 5 with markers of the same size in order to compare them. It can be seen, Fig. 5a, b, that surface samples of Ni-0 and Ni-2 electrodes exhibit sponge-like structures with defined holes or porous. The results in Fig. 5c, d exhibit that with increasing the nanomaterial content in the electrodes (Ni-5 and Ni-10), a more compact surface morphology is observed. These facts indicate that the increment (5 and 10 %) of the nickel hydroxide nanoparticles content, employed in the sample preparation, is responsible for these surface morphologies changes.

Electrochemical behavior

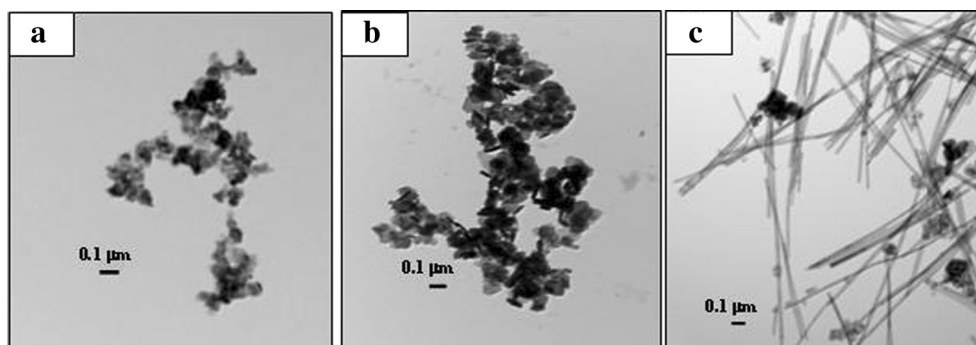
Figure 6 depicts the stabilized cyclic voltammetry profiles of working electrodes. The voltammograms show the CV peaks corresponding to a redox process, an anodic nickel hydroxide oxidation peak, and a cathodic oxyhydroxide reduction peak, which are described as:



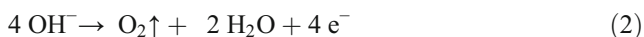
The electrochemical energy storage in the nickel hydroxide electrodes is related to the reversible insertion of H⁺ into the nickel hydroxide/oxyhydroxide. The insertion of the hydrogen takes place during the discharge and the inverse process occurs during the charge. Accordingly, the reversibility of this process is an important requirement for battery electrode materials.

Figure 6 shows the anodic peak potentials (E_a) of the studied samples, corresponding to nickel hydroxide oxidation reaction (Eq. 1). The cathodic peak potentials (E_c) in Fig. 6 are related to nickel oxyhydroxide reduction (Eq. 1) and they appear at around 0.28 V for Ni-0 and Ni-2 electrodes. In the samples containing higher amounts of nickel hydroxide nanoparticles (Ni-5 and Ni-10 electrodes), reduction peaks are broader and appear to be located at more positive potentials (0.360 V). The difference between the anodic and cathodic peak potentials ($\Delta E_{a,c}$) is an indication of the reversibility of the redox process described in reaction (1). Accordingly (Table 2), the smaller $\Delta E_{a,c}$ ($\cong 0.100$ V) values exhibited for electrodes containing higher amount of nickel hydroxide nanoparticles (5 and 10 %) indicate the enhancement of reversibility for this redox reaction.

Fig. 4 TEM images of β -nickel hydroxide prepared by the hydrothermal method at **a** 4, **b** 12, and **c** 24 h



For all samples, the oxidation reaction appears to be overlapped by the oxygen evolution reaction expressed by equation:



The oxygen evolution reaction is a parasitic reaction that causes the decrease in charging efficiency, in the energy storage capacity of the system, and in the utilization of the active material.

Discharge curves of the studied electrodes, which correspond to the 10th cycle at 0.5 C rate, are illustrated in Fig. 7. For samples containing nickel hydroxide nanoparticles, the potential related to a plateau appear as not very well defined. These results, along with those from cyclic voltammetry profiles (Fig. 6), could be understood taking into consideration that particle sizes may affect the different components of the electrochemical potential [6].

The specific discharge capacity curves, of the studied working electrodes, at various constant current densities are presented in Fig. 8. These results exhibit a significant improvement of the specific discharge capacity values with increasing the nanomaterial percentage. The maximum specific discharge capacity values (obtained from extrapolation to $I = 0$) were found to be around 69, 77, 85, and 88 mA h g⁻¹ for Ni-0, Ni-2, Ni-5, and Ni-10 electrodes, respectively. These experimental results show that the increase of nano-nickel hydroxide addition from 2 to 10 % enhances the maximum specific discharge capacity values of electrodes from 11 to 27 %.

The electrochemical impedance spectra of working electrodes, at 60 % SOD, are shown in Fig. 9. The enlargement of these plots in the high-frequency range (inserted in Fig. 9a) shows a linear response of the impedance results with a slope of approximately 45° associated with the surface properties of porous electrodes [34]. The spectra exhibit at the intermediate range of frequencies, the capacitive loop that corresponds to the charge transfer resistance. In the low frequency domain, the plot shows, for Ni-0 electrodes, a Warburg-type impedance [35–37]. However, for nickel electrodes containing nanomaterials, the impedance results show a distorted response compared with that related to the characteristic features of diffusional impedances.

It can be seen that, when the composition of electrodes includes nano-nickel hydroxide material, the impedance values, mainly at high and intermediate frequency ranges (Fig. 9b), are higher than that corresponding to Ni-0. These results (Fig. 9a, b) indicate response modifications in the frequency domain related to the porous nature of the electrodes as well as in that associated with the charge transfer resistance processes.

The EIS response of the nickel electrode was fitted in terms of a modified version of the physicochemical model that has been described in previous publications [8, 11, 13, 20–22]. Briefly, the previous model considered the electrodes as porous flooded structures where the electrochemical processes take place at the active material/electrolyte interface, this process being coupled to the proton diffusion in the active material (reaction 1). Accordingly, the theoretical impedance of the

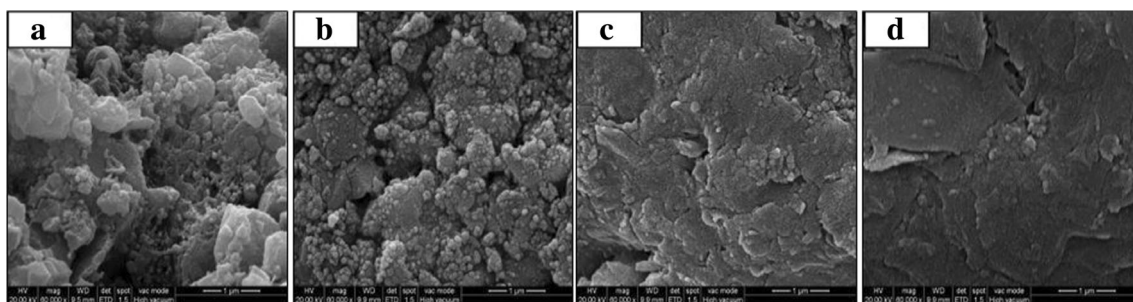


Fig. 5 SEM micrographs for **a** Ni-0, **b** Ni-2, **c** Ni-5, and **d** Ni-10 electrodes

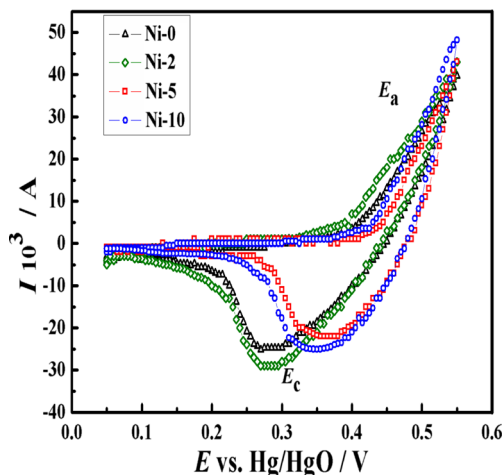


Fig. 6 Cyclic voltammograms for working electrodes at 5 mV s⁻¹

system is described by the impedance of the porous electrode per unit geometric area (Z_p):

$$Z_p(j\omega) = \frac{L}{A_p(\kappa + \sigma)} \left[1 + \frac{2 + \left(\frac{\sigma}{\kappa} + \frac{\kappa}{\sigma}\right) \cosh \nu(j\omega)}{\nu(j\omega) \sinh \nu(j\omega)} \right]$$

where

$$\nu(j\omega) = L \left(\frac{\kappa + \sigma}{\kappa \sigma} \right)^{1/2} Z_i^{-1/2}(j\omega)$$

L being the electrode thickness, A_p the electrode geometric area (cross section), κ and σ the effective conductivities of the liquid and solid phases, respectively, and Z_i the impedance of the solid/liquid interface per electrode unit volume ($\Omega \text{ cm}^3$). The interfacial impedance (Z_i) is derived considering the double-layer capacitance impedance (Z_{dl}) linked in parallel with the faradaic reaction impedance (Z_F).

$$Z_i^{-1} = Z_{dl}^{-1} + Z_F^{-1}$$

where

$$Z_{dl} = \frac{1}{j\omega C_{dl} a_e}$$

$j = \sqrt{-1}$; being the C_{dl} double-layer capacitance per unit interfacial area, a_e the interfacial area per unit volume (cm^{-1}), and $\omega = 2\pi f$ (f , frequency of the perturbing signal (Hz)).

Table 2 Potential peak values of CV measurements

Electrode	E_a (V)	E_c (V)	$\Delta E_{a,c}$ (V)
Ni-0	≈0.450	0.280	0.170
Ni-2	≈0.450	0.280	0.170
Ni-5	≈0.470	0.360	0.110
Ni-10	≈0.470	0.360	0.110

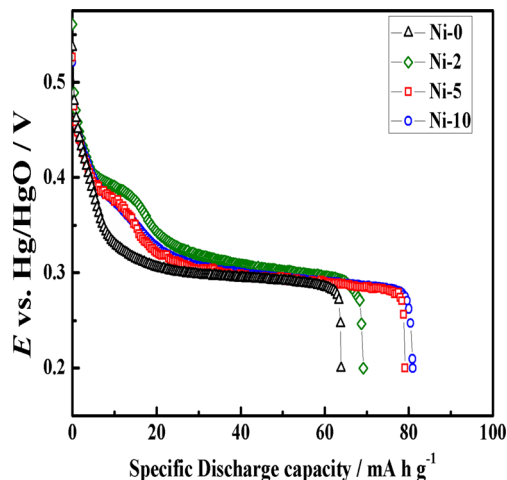


Fig. 7 Discharge profiles of nickel electrodes at 0.5 C

According to the previously described physicochemical model [8, 11, 13, 20–22], Z_F is represented by a Warburg-type impedance as:

$$Z_F(j\omega) = \frac{Z_f}{a_a} = \frac{R_t}{a_a} + \frac{A}{a_a \sqrt{j\omega}} = \frac{RT}{i_0 F a_a} + \frac{RT}{F^2 \text{SOD}(1-\text{SOD}) c_m a_a \sqrt{D} \sqrt{j\omega}}$$

where Z_f is related to the faradaic impedance per unit interfacial area ($\Omega \text{ cm}^2$), a_a is the active area per unit volume (cm^{-1}), SOD accounts for the state of discharge of the electrode, c_m corresponds to maximum admitted proton concentration, i_0 is the exchange current density, and D is the proton diffusion coefficient.

In the present work, the impedance function for the samples containing nano-nickel hydroxide (Ni-2, Ni-5 and Ni-10 electrodes) was derived. The modified model considers the presence of two particle sizes and different diffusion coefficient values related to each material. Accordingly,

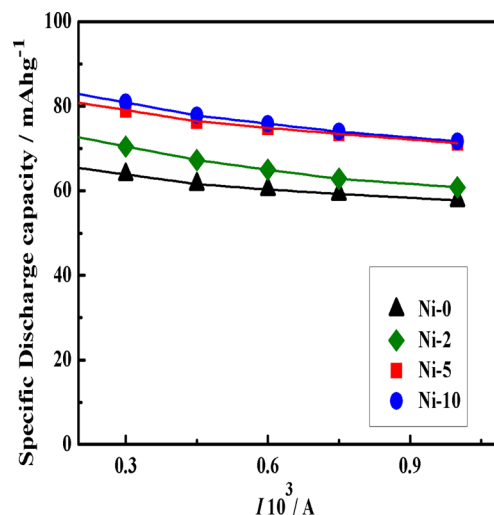
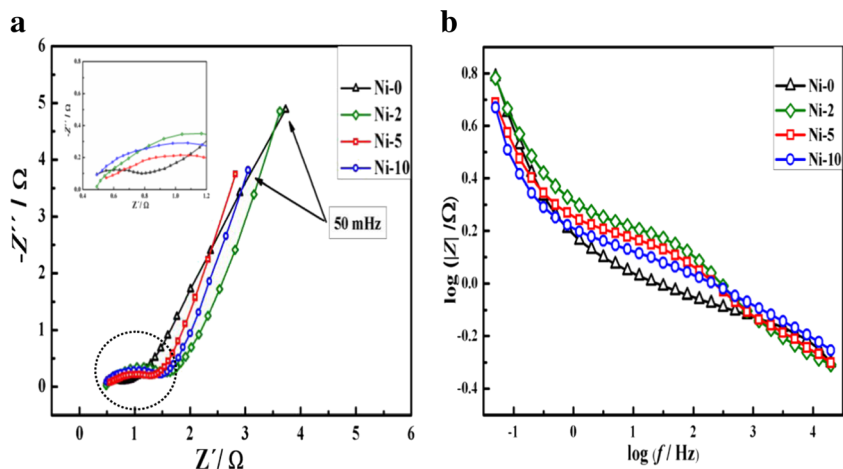


Fig. 8 Rate performances of nickel electrodes in 7 M KOH electrolyte

Fig. 9 Experimental electrochemical impedance spectrum of working electrodes at 60 % SOD **a** Nyquist plots and **b** Bode plots



$$\begin{cases} Z_F = \frac{Z_f}{a_a} \rightarrow \text{when one particle size of active material is considered} \\ \hspace{1.5cm} \text{(Ni-0 electrode)} \\ Z_F = \frac{Z_{f1}}{a_{a1}} + \frac{Z_{f2}}{a_{a2}} \rightarrow \text{when two particle sizes in the active material are considered} \\ \hspace{1.5cm} \text{(Ni-2 and Ni-10 electrodes)} \end{cases}$$

To perform parameter identifications, a fitting program based on the Nelder-Mead simplex search algorithm, included in the Matlab package, was developed.

The minimized objective function during the fitting procedure was the cost function J_p [21]. The fitting was considered acceptable when $J_p < 5 \cdot 10^{-3}$.

The experimental EIS spectra are compared with the fitted EIS results obtained considering the above-described

physicochemical model. Therefore, Fig. 10 shows that a fairly good agreement between experimental and fitted results was obtained.

The characteristic parameters derived from the fitting procedure are listed in Table 3 for a constant SOD: the double-layer capacitance per unit volume (C_{dl}), the exchange current density (i_0), the diffusion coefficient of hydrogen according to materials with different particle sizes (D_1 and D_2), and the effective electrolyte conductivity values (κ). The results in Table 3 show that electrodes containing nano-nickel hydroxide (Ni-2, Ni-5, and Ni-10 electrodes) present higher diffusion coefficient values (D_2), related to smaller-size particle materials. These facts are in agreement with reported data for

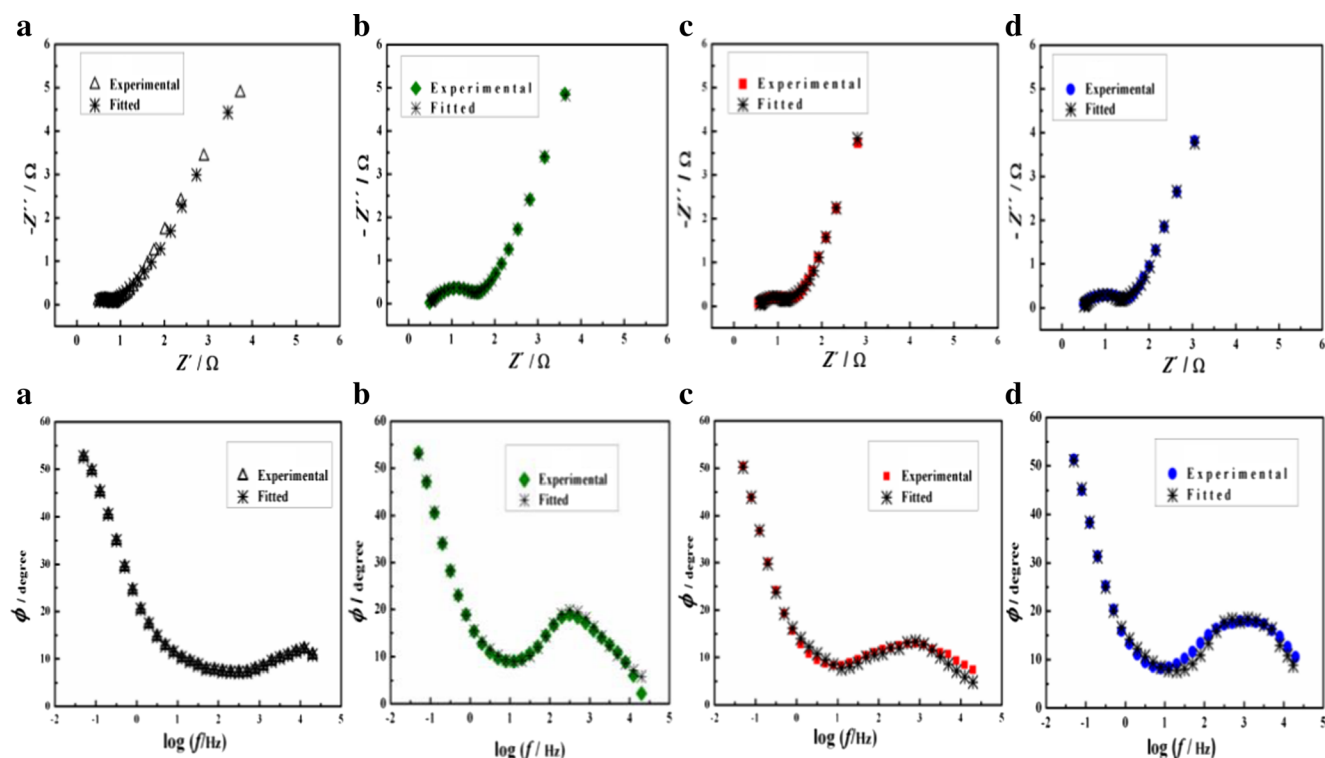


Fig. 10 Experimental and theoretical impedance plots for **a** Ni-0 electrode, **b** Ni-2 electrode, **c** Ni-5 electrode, and **d** Ni-10 electrode

Table 3 Estimated structural and physicochemical parameters

Electrode	SOD	$D_1/\text{cm}^2 \text{ s}^{-1}$ ($\pm 0.02 \cdot 10^{-13}$)	$D_2/\text{cm}^2 \text{ s}^{-1}$ ($\pm 0.02 \cdot 10^{-11}$)	$i_0/\text{A cm}^{-2}$ ($\pm 9 \cdot 10^{-5}$)	$\kappa/\Omega^{-1} \text{ cm}^{-1}$ (± 0.001)	$C_{dl}/\text{F cm}^{-3}$ (± 0.003)
Ni-0	60	$9.20 \cdot 10^{-13}$	–	$2.1 \cdot 10^{-4}$	0.217	0.091
Ni-2	60	$8.11 \cdot 10^{-13}$	$1.02 \cdot 10^{-11}$	$3.9 \cdot 10^{-4}$	0.174	0.077
Ni-5	60	$9.30 \cdot 10^{-13}$	$3.07 \cdot 10^{-11}$	$3.8 \cdot 10^{-4}$	0.092	0.057
Ni-10	60	$9.31 \cdot 10^{-13}$	$2.80 \cdot 10^{-11}$	$3.6 \cdot 10^{-4}$	0.081	0.069

nanomaterials [2–5, 7]. Besides, Table 3 shows that C_{dl} and κ values diminish with an increasing percent of nano-nickel hydroxide. These results could be explained taking into consideration that more-compact (lower active area) and less-porous systems (porosity factor is contained in the κ value [21]) are formed in the presence of nano-nickel hydroxide powders. These facts are in good agreement with SEM results (Fig. 5).

Furthermore, for Ni-2, Ni-5, and Ni-10 samples, higher values of the exchange current density parameter than that corresponding to Ni-0 electrodes were estimated (Table 3). This can be understood taking into account that the size, morphology, and dispersion of the surface particles can influence the reactivity of the sites [38].

According to the estimated characteristic parameters, derived from the physicochemical model, the significant improvement of the maximum specific discharge capacity (from 11 up to 27 %) with increasing the nanomaterial percentage (Fig. 8) can be attributed to their higher kinetic parameters such as diffusion coefficient and exchange current density values (Table 3). Furthermore, it is considered that the optimum compromise between interfacial area (to ensure high capacitance) and porosity distribution (to allow easy access to the electrolyte) remains as a challenge to be addressed. A similar study employing nano-nickel hydroxide as additive, with greater particle sizes (i.e., β -Ni(OH)₂-12), is in progress.

Conclusions

In summary, a nano-nickel hydroxide material was synthesized via a facile and single-step hydrothermal method and characterized by XRD, IR, and TEM.

Considering all the results, greater reversibility of the redox process Ni(OH)₂/NiOOH and better capacity responses were obtained with electrodes containing at least 5 wt.% of nano-nickel hydroxide. The experimental results show that the increase of nano-nickel hydroxide addition, from 2 to 10 %, enhances the maximum specific discharge capacity values of electrodes from 11 to 27 %. The analysis of EIS results, according to the present physico-mathematical model, allows estimating the main structural and physicochemical parameters that control the electrochemical performance of these systems. Accordingly, the specific discharge capacity improvement, of Ni-2, Ni-5, and Ni-

10 electrodes, can be attributed to their higher kinetic parameters: diffusion coefficient and exchange current density values.

Acknowledgments The authors would like to acknowledge the financial support from the Agencia Nacional de Promoción Científica y Tecnológica (ANPCyT), Consejo Nacional de Investigaciones Científicas y Técnicas (CONICET), and Universidad Tecnológica Nacional (UTN).

References

- Liu X, Yu L (2004) Synthesis of nanosized nickel hydroxide by solid-state reaction at room temperature. *Mater Lett* 58:1327–1330
- Liu X, Yu L (2004) Influence of nanosized Ni(OH)₂ addition on the electrochemical performance of nickel hydroxide electrode. *J Power Sources* 128:326–330
- Han XJ, Xu P, Xu CQ, Zhao L, Mo ZB, Liu T (2005) Study of the effects of nanometer β -Ni(OH)₂ in nickel hydroxide electrodes. *Electrochim Acta* 50:2763–2769
- Kiani MA, Mousavi MF, Ghasemi S (2010) Size effect investigation on battery performance: comparison between micro- and nanoparticles of β -Ni(OH)₂ as nickel battery cathode material. *J Power Sources* 195:5794–5800
- Jiang Q, Zhang SH, Li JC (2004) Grain size-dependent diffusion activation energy in nanomaterials. *Solid State Commun* 130:581–584
- Balaya P, Bhattacharyya AJ, Jamnik J, Zhukovskii YF, Kotomin EA, Maier J (2006) Nano-ionics in the context of lithium batteries. *J Power Sources* 159:171–178
- Bruce PG, Scrosati B, Tarascon J-M (2008) Nanomaterials for rechargeable lithium batteries. *Wiley-VCH Verlag GmbH & Co. KGaA, Weinheim. Angew Chem Int Ed* 47:2930–2946
- Ortiz MG, Real SG, Castro EB (2014) Preparation and characterization of positive electrode of Ni-MH batteries with cobalt additives. *Int J Hydrog Energy* 39:8661–8666
- Provazi K, Giz MJ, Dall' Antonia LH, Córdoba de Torresi SI (2001) The effect of Cd, Co, and Zn as additives on nickel hydroxide opto-electrochemical behaviour. *J Power Sources* 102:224–232
- Watanabe K, Koseki M, Kumagai N (1996) Effect of cobalt addition to nickel hydroxide as a positive material for rechargeable alkaline batteries. *J Power Sources* 58:23–28
- Ortiz MG, Castro EB, Real SG (2014) Effect of cobalt electroless deposition on nickel hydroxide electrodes. *Int J Hydrog Energy* 39:6006–6012
- Martins PR, Araújo Parussulo AL, Hiroshi Toma S, Rocha MA, Eisi Toma H, Arak K (2012) Highly stabilized alpha-NiCo(OH)₂ nanomaterials for high performance device application. *J Power Sources* 218:1–4
- Ortiz MG, Castro EB, Real SG (2016) Electrochemical characterization of MWCNT/Ni(OH)₂ composites as cathode materials. *J Solid State Electrochem* 20(4):1029–1036

14. Liu B, XY W, HT Y, YS Z, DY S, ZX Z (1999) Physical and electrochemical characteristics of aluminium-substituted nickel hydroxide. *J Appl Electrochem* 29:853–858
15. Hu WK, Gao XP, Geng MM, Gong ZX, Noréus D (2005) Synthesis of CoOOH nanorods and application as coating materials of nickel hydroxide for high temperature Ni-MH cells. *J Phys Chem B* 109: 5392–5394
16. Li WY, Zhang S, Chen J (2005) Synthesis, characterization, and electrochemical application of Ca(OH)₂-, Co(OH)₂-, and Y(OH)₃-coated Ni(OH)₂ tubes. *J Phys Chem B* 109:14025–14032
17. Jiao Q-Z, Tian Z-L, Zhao Y (2007) Preparation of nickel hydroxide nanorods/nanotubes and microscopic nanoring under hydrothermal conditions. *J Nanopart Res* 9:519–522
18. Yang L-X, Zhu Y-J, Tong H, Liang Z-H, Liang L, Zhang L (2007) Hydrothermal synthesis of nickel hydroxide nanostructures in mixed solvents of water and alcohol. *J Solid State Chem* 180:2095–2101
19. Kong X, Liu X, He Y, Zhang D, Wang X, Li Y (2007) Hydrothermal synthesis of β -nickel hydroxide microspheres with flakelike nanostructures and their electrochemical properties. *Mater Chem Phys* 106:375–378
20. Castro EB, Cuscueta DJ, Milocco RH, Ghilarducci AA, Salva HR (2010) An EIS based study of a Ni-MH battery prototype. Modeling and identification analysis. *Int J Hydrog Energy* 35:5991–5998
21. Ortiz MG, Becker D, Garaventa G, Visintin A, Castro EB, Real SG (2011) Dynamic monitoring of structural changes in nickel hydroxide electrodes during discharge in batteries. *Electrochim Acta* 5: 7946–7954
22. Ortiz MG, Castro EB, Real SG (2012) The cobalt content effect on the electrochemical behavior of nickel hydroxide electrodes. *Int J Hydrog Energy* 37:10365–10370
23. Li Y, Yao J, Zhu Y, Zou Z, Wang H (2012) Synthesis and electrochemical performance of mixed phase α/β nickel hydroxide. *J Power Sources* 203:177–183
24. Ramesh TN, Vishnu Kamath P (2008) The effect of stacking faults on the electrochemical performance of nickel hydroxide electrodes. *Mater Res Bull* 43:2827–2832
25. Delmas C, Tessier C (1997) Stacking faults in the structure of nickel hydroxide: a rationale of its high electrochemical activity. *J Mater Chem* 7:1439–1443
26. Tessier C, Guerlou-Demourgues L, Faure C, Basterreix M, Nabias G, Delmas C (2000) Structural and textural evolution of zinc-substituted nickel hydroxide electrode materials upon ageing in KOH and upon redox cycling. *Solid State Ionics* 133:11–23
27. Ramesh TN (2009) Crystallite size effects in stacking faulted nickel hydroxide and its electrochemical behaviour. *Mater Chem Phys* 114:618–623
28. Guerlou-Demourgues L, Tessier C, Bernard P, Delmas C (2004) Influence of substituted zinc on stacking faults in nickel hydroxide. *J Mater Chem* 14:2649–2654
29. Bernard MC, Cortes R, Keddam M, Takenouti H, Bernard P, Senyari S (1996) Structural defects and electrochemical reactivity of β -Ni(OH)₂. *J Power Sources* 63:247–254
30. Patterson AL (1939) The Scherrer formula for X-ray particle size determination. *Phys Rev* 56:978–982
31. Nathira Begum S, Muralidharan VS, Ahmed Basha C (2009) The influences of some additives on electrochemical behaviour of nickel electrodes. *Int J Hydrog Energy* 34:1548–1555
32. Wang X, Luo H, Parkhutik PV, Millan A-C, Matveeva E (2003) Studies of the performance of nanostructural multiphase nickel hydroxide. *J Power Sources* 115:153–160
33. Shruthi B, Bheema Raju V, Madhu BJ (2015) Synthesis, spectroscopic and electrochemical performance of pasted β -nickel hydroxide electrode in alkaline electrolyte. *Spectrochim Acta A Mol Biomol Spectrosc* 135:683–689
34. De Levie R (1967) In: Delahay P (ed) *Advances in electrochemistry and electrochemistry engineering*, 6. Interscience, NY, pp. 329–361
35. Ho C, Raistrick ID, Huggins RA (1980) Application of A-C techniques to the study of lithium diffusion in tungsten trioxide thin films. *J Electrochem Society* 127:343–350
36. Jacobsen T, West K (1995) Diffusion impedance in planar, cylindrical and spherical symmetry. *Electrochim Acta* 40:255–262
37. Barsoukov E, Macdonald JR (2005) *Impedance spectroscopy: theory, experiment, and applications*, 2nd edn N.J. Wiley-Interscience, Hoboken
38. Arico AS, Bruce P, Scrosati B, Tarascon J-M, Van Schalkwijk W (2004) Nanostructured materials for advanced energy conversion and storage devices. *Nat Mater* 4:366–377